

Analysis of Pointing Errors Reveals Properties of Data Representations and Coordinate Transformations Within the Central Nervous System

J. McIntyre

Scientific Institute S. Lucia, National Research Council, University of Rome Tor Vergata Rome, Italy, and Laboratoire de Physiologie de la Perception et de l'Action, Centre National de la Recherche Scientifique, Collège de France, Paris, France

F. Stratta

Scientific Institute S. Lucia, National Research Council, University of Rome Tor Vergata, Rome, Italy

J. Droulez

Laboratoire de Physiologie de la Perception et de l'Action, Centre National de la Recherche Scientifique, Collège de France, Paris, France

F. Lacquaniti

Scientific Institute S. Lucia, National Research Council, University of Rome Tor Vergata Rome, Italy

The execution of a simple pointing task invokes a chain of processing that includes visual acquisition of the target, coordination of multimodal proprioceptive signals, and ultimately the generation of a motor command that will drive the finger to the desired target location. These processes in the sensorimotor chain can be described in terms of internal representations of the target or limb positions and coordinate transformations between different internal reference frames. In this article we first describe how different types of error analysis can be used to identify properties of the internal representations and coordinate transformations within the central nervous system. We then describe a series of experiments in which subjects pointed to remembered 3D visual targets under two lighting conditions (dim light and total darkness) and after two different memory delays (0.5 and 5.0 s) and report results in terms of variable error, constant error, and local distortion. Finally, we present a set of simulations to help explain the patterns of errors produced in this pointing task. These analyses and experiments provide insight into the structure of the underlying sensorimotor processes employed by the central nervous system.

1 Introduction

Assessment of errors in pointing toward visual targets has long been used to study the neural control of movement. Sherrington (1918), and later Merton (1961), used observations about eye movement accuracy to argue for or against a role of eye muscle proprioception in oculomotor control. Merton recognized the importance of measuring response variability (*variable error*), rather than mean error (*constant error*), to assess the performance of the sensory motor chain. More recently, analyses of constant and variable pointing errors have been used to identify the sources of information that contribute to the internal representation of a memorized target position (Foley & Held, 1972; Prablanc, Echallier, Komilis, & Jeannerod, 1979; Poulton, 1981; Soechting & Flanders, 1989a; Darling & Miller, 1993; Berkinblit, Fookson, Smetanin, Adamovich, & Poizner, 1995; Desmurget, Jordan, Prablanc, & Jeannerod, 1997; Baud-Bovy & Viviani, 1998; McIntyre, Stratta, & Lacquaniti, 1997, 1998; Lacquaniti, 1997). Recently, we have proposed a third measure of pointing errors, called the *local distortion*, which we have used to characterize neural mechanisms involved in pointing to visually presented 3D targets. In this article, we set out to formalize the relationship of these three different measures of pointing error. We then apply these measures to the analysis of errors observed in a 3D pointing experiment (the data have been previously reported in McIntyre et al., 1998). Finally, through a set of simulations, we show how the analysis of pointing errors can contribute to the understanding of the neural processes involved in pointing.

2 Local Distortion

As a complement to the standard measures of constant and variable errors, we propose an additional measure, which we call *local distortion*. Local distortion describes the mapping of spatial relationships between nearby points as data are transformed between coordinate systems. Consider a circular array of targets (see Figure 1a, open circles). The mean position of repeated movements to each target creates an array of final pointing positions (filled circles in Figure 1). If the sensorimotor transformation is accurate, the array of mean final positions should reproduce exactly the spatial relationships between the individual targets of the array. The measurement of local distortion refers to the fidelity with which the relative spatial organization of the targets is maintained in the configuration of final pointing positions, independent of displacement of the entire array. If the constant error in the mapping from target to end point position is the same for all eight targets, the array of final pointing positions will be an undistorted replica of the target array, even though it may be displaced by a large, constant error common to all targets (see Figure 1b). On the other hand, differences in the mapping of individual targets can result in a distorted representation of the target array within the pattern of final pointing positions. This dis-

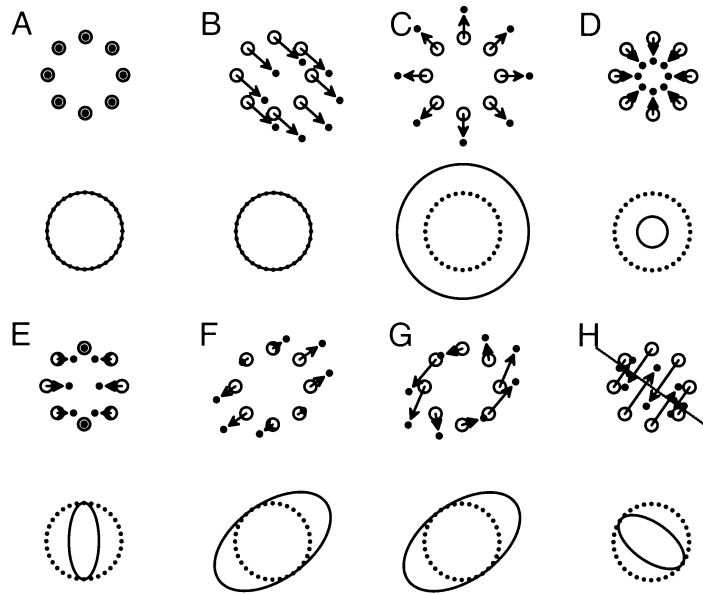


Figure 1: Definition of local distortion. An undistorted representation of the relative target positions is reproduced in the final pointing positions (closed circles) if errors in transformations are absent (A) or restricted to biases common to all targets (B). Distorted end point configurations may be produced by inaccurate transformations, resulting in expansion (C), contraction (D), anisotropic expansion and/or contraction (E, F). Rotations (G) or reflections (H) may also appear, with or without accompanying expansion or contraction.

Distortion can manifest itself as an expansion or contraction of the local space (see Figures 1c and 1d), and the expansion or contraction may be unequal for different dimensions, resulting in an anisotropic distortion of the target array (see Figures 1e and 1f). The transformation from target to end point position might also include a rotation or reflection of the local space, either alone or in combination with local expansion or contraction (see Figures 1g and 1h).

The transformation from target to final pointing position will in general be a nonlinear process in which the binocularly acquired target position is transformed into an appropriate joint posture. For a small area of the workspace, however, one would expect the transformation to be continuous and smooth. In this case, local distortions of the spatial organization of the targets can be approximated by a linear transformation from target to end point position. Such linear approximations can be described by a transformation matrix, which can be presented graphically as an oriented ellipse (ellipsoid in 3D). Figures 1a–1h show the representation of each type

of distortion as an ellipse. The ellipse encompasses the area that would be occupied by a circular array of targets after passage through the transformation. Note that an ellipse cannot be used to indicate or assess the presence of rotations or mirror reflections within the local transformation. The ellipses in Figures 1f and 1g, for instance, are identical, although they result from two different distorted transformations. However, if the absence of rotations or reflections in the local transformation can be demonstrated independently, the graphical presentation of the local transformation as an ellipse provides an intuitive and unambiguous visual representation of local distortions in the mapping from target to end point positions.

3 Sources of Error

Conceptually, one can identify two distinct components in the processes leading from target localization to end point specification during a reaching or pointing task: (1) internal representations of the target location and (2) transformations of information between internal representations. For instance, the encoding of a target's projection on the retina, the eyes' position in the orbit, and the head's position with respect to the trunk all constitute potential internal representations, while the combination of these three sources of information into a (hypothetical) representation of the target location with respect to the body would involve a coordinate transformation. The three measures of error defined above can be used to identify the characteristics of these different components within a sensorimotor pathway.

Consider, for example, an idealized system that converts a 2D Cartesian target location into an internal polar representation, then back into a 2D Cartesian end point position (see Figure 2). In this hypothetical system, we have three representations of the target position (the Cartesian input and output plus the polar intermediate representation) and two coordinate transformations. By tracking the effects of bias, noise, and distortions as information passes through this system, one can see how each of these effects can be observed in measurements of error at the output and, conversely, how measurements of error at the output can be used to identify the internal structure of the system.

3.1 Bias. The observation of constant errors at the output of a sensorimotor transformation suggests the presence of bias in an internal representation of the target position or motor command. Patterns of constant error might therefore indicate the coordinate system of the biased internal representation. If the bias is assumed to occur in only one channel of a given coordinate system (an unlikely assumption), the patterns of constant error seen for different workspace regions would indicate the orientation of that internal coordinate system with respect to the world. For example, a constant bias in the estimated distance of the target position would generate a radial pattern of constant errors in the final pointing positions (see Fig-

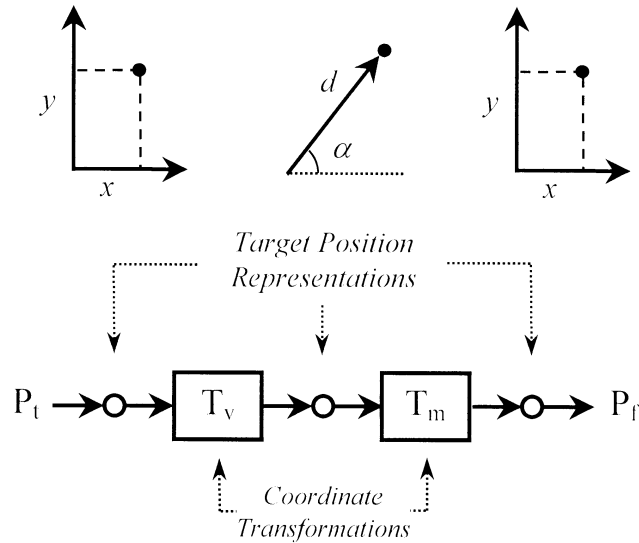


Figure 2: Model system for demonstrating the relationship between variable error, constant error, and local distortions. The model converts a 2D target position into an internal polar representation, then back to a 2D Cartesian pointing position.

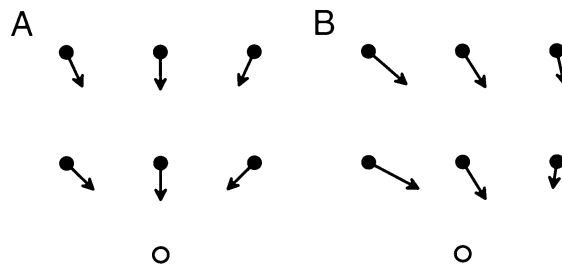


Figure 3: (A) Pattern of constant error (undershoot) for pointing to six different targets (closed circles) induced by a fixed bias in the estimate of target distance. Constant errors (arrows) point toward the origin (open circle) of the polar coordinate system. (B) Pattern of constant error induced by a fixed bias in both the target distance and along the x-axis in the output stage. In this case, the constant error vectors do not point directly toward the origin of the internal polar representation, but rotate around the y-axis.

ure 3A). The existence of such a pattern of errors would therefore provide evidence for the internal polar representation of our model system. Furthermore, the constant error vectors would point to the origin of the polar

coordinate frame. However, bias is not likely to be restricted to a single coordinate axis, and biases in different coordinate frames can add, resulting in a potentially confusing array of constant errors in the workspace (see Figure 3B). Nevertheless, if biases in the system depend on only the workspace location, rotation of the constant error vectors around a single workspace axis would still argue for an internal polar representation of the target position. Parallel constant errors, on the other hand, would indicate a Cartesian representation that for our model system would correspond to bias in either the input or output stages.

3.2 Random Noise. The measurement of the variable error can detect the presence of random noise added at any of the stages of a sensorimotor transformation and thus reveal features of the internal representation of the target location or intended movement. Random noise should be statistically independent between two truly separate channels of information. If the level of noise is greater in one channel than another, the eigenvectors of the covariance matrix will indicate the directions of maximal and minimal variance, and if the two channels are orthogonal, they will thus reveal the local spatial orientation of the underlying independent channels. Changing patterns of variable error across different workspace regions can indicate the existence and the origin of an internal data representation. For instance, in our model system, a greater level of variability in the estimate of target distance versus direction¹ would result in a radial pattern of variable error eigenvectors, as seen in Figure 4a.

In a multistage transformation, noise added at different stages in the sensorimotor chain may add to form complex patterns of variability at the output. The orientation of anisotropic noise at the output will depend on the relative magnitude of noise at the different intermediate stages. For instance, the radial pattern of variable error produced by noise in the polar representation will become progressively more parallel in the vertical direction as more and more noise is added to the Y channel in the output stage (see Figures 4d and 4g). Adding noise to the X output channel will cause the variable error ellipses to widen, ultimately resulting in ellipses that are horizontally oriented (see Figure 4c). This occurs after passing through a point where anisotropy in the polar and Cartesian representations cancels to generate isotropic output noise (see Figure 4b, near center position). Adding isotropic noise at the output will cause the ellipses to expand in all directions while having a minimal effect on the orientation of the major eigenvector (see Figure 4e), until the isotropic output noise dominates and the output variability becomes essentially circular (see Figure 4i).

¹ Although one cannot in general compare variability of target distance, measured in mm, with the variable error of target direction, measured in degrees, one can compare the effect of a given noise level in each channel on the Cartesian position of the output at a given nominal distance.

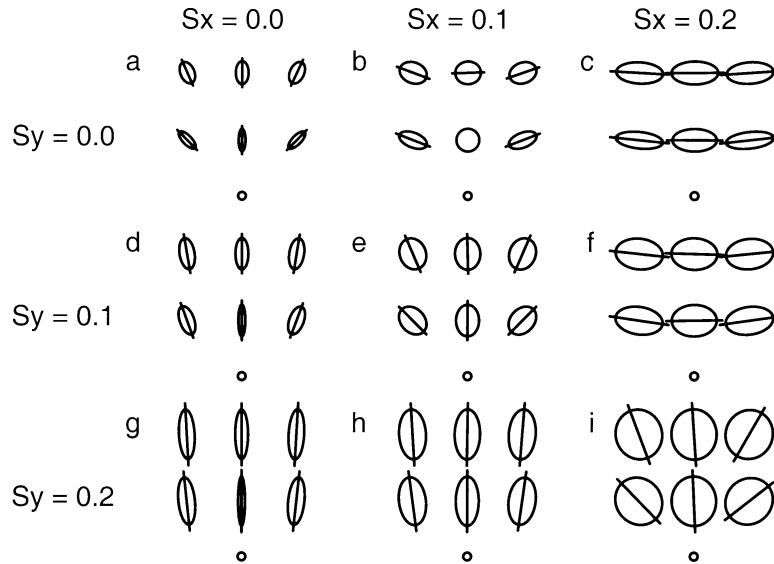
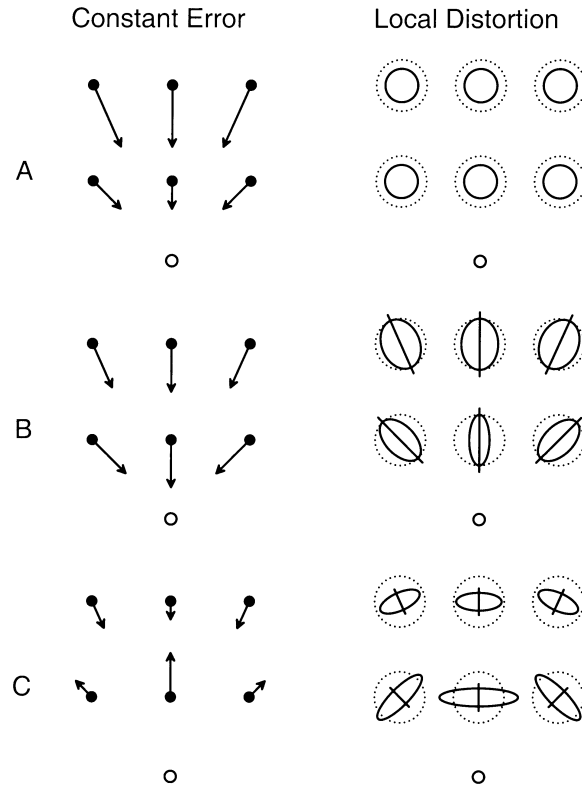


Figure 4: Patterns of variable error expected from an independent estimate of target distance and direction, plus variable levels of noise in X and Y at the output. Black bars in plots of variable error indicate the axis of maximum variability. Anisotropy is apparent in the variable-error ellipse, despite accurate transformations between coordinate systems. Noise in the polar representation of distance and direction generates a radial pattern of variable errors (a). Increasing variability in X (b, c) or Y (d, g) in addition to the noise in distance and direction causes variable errors to align gradually with the x- or y-axis, respectively. The addition of isotropic noise ($\sigma_x = \sigma_y$; e, i) changes the size but not the orientation of the variable-error ellipsoids.

3.3 Distortion. Errors in transformations between coordinate systems can lead to distortions in the mapping from target locations to pointing positions. Consider, for example, an output transformation in which the distance to the target is improperly computed:

$$\begin{aligned}
 P_f^x &= f(d) \cos \alpha \\
 P_f^y &= f(d) \sin \alpha,
 \end{aligned}
 \tag{3.1}$$

where P_f^x and P_f^y represent the Cartesian coordinates of the end point, d and α are the internal representation of the distance and direction to the target, respectively, and $f(d)$ represents the distorted computation of distance in the transformation from polar to Cartesian coordinates. If the distorted distance



is simply a scaled representation of the true distance,

$$f(d) = \lambda d, \quad (3.2)$$

the output pointing positions will result in a systematic pattern of radial constant errors that increase with the distance from the origin and isotropic contraction ($\lambda < 1$) or expansion ($\lambda > 1$) of relative pointing positions that can be quantified by the measurement of local distortion (see Figure 5A).

Bias, which we have previously considered to be a property of a data representation, may in fact be due to an erroneous coordinate transformation. The addition of bias in the output of a transformation will not in itself change the local spatial organization of the output and as such should not be considered as a case of local distortion. In our model system, the addition of bias in the Cartesian output would generate a shift (constant error) of all output positions, but would not affect the relative spatial organization between targets. On the other hand, the addition of bias to an intermediate

representation, followed by a second nonlinear transformation, can lead to local distortion in the output. For instance, in our model system, bias added to the internal representation of target distance,

$$f(d) = d + \gamma, \quad (3.3)$$

creates not only a radial pattern of constant error but also an anisotropic contraction ($\gamma < 0$) or expansion ($\gamma > 0$) of the relative pointing positions that depends on the distance from the origin (see Figure 5B).

The combination of both scaling and offset errors,

$$f(d) = \lambda d + \gamma, \quad (3.4)$$

leads to a more complicated pattern of constant error and local distortion at the output. Both undershoot and overshoot may appear in the radial pattern of constant errors. For $\lambda < 1$, this type of error will also manifest itself as an anisotropic contraction along radially oriented axes (see Figure 5C), but there will be lateral expansion or contraction depending on whether there is overshoot or undershoot for a particular workspace region. In this example, the orientation of both the constant error and the local distortion ellipse would indicate a property of the erroneous coordinate transformation. Of course, other nonlinear distortions of the estimated target distance might also introduce anisotropic distortions at the output. But to the extent that well-behaved (i.e., continuous and smooth) transformations can be locally approximated by a linear function, the ellipses in Figure 5C are representative of the types of local distortion that might be observed in a real sensorimotor chain.

Figure 5: *Facing page*. Patterns of constant error and local distortion induced by incorrect estimates of target distance in the transformation from polar to Cartesian coordinates. Dotted circles indicate an undistorted transformation for reference, while solid circles and ellipses indicate the local distortion for a given workspace region. (A) For a proportional underestimation of target distance (see equation 3.2), constant errors point inward, and local distortion indicates isotropic contraction. (B) A constant undershoot in the estimate of target distance (see equation 3.3) will evoke both a radial pattern of constant errors and anisotropic contraction perpendicular to the radial axis (black bars). (C) Contraction and bias in estimated target distances or contraction toward an average distance (see equation 3.4) may yield both overshoot and undershoot in measures of constant error. Measurements of local distortion show anisotropic contraction along a radial axis toward the origin of the polar coordinate system, as indicated by the dark bars (eigenvector corresponding to the smallest eigenvalue). Local distortion may indicate lateral expansion or contraction, depending on whether the target distance is over- or underestimated in a given region.

One can see from these examples that measurements of constant error and local distortion are closely related. Both arise from errors in transformations. Figure 5C demonstrates, however, that the measurement of local distortion complements the classical assessment of constant error; computing both may lead to a better understanding of the underlying neural mechanisms. In the next section we describe how measurements of local distortion can also be useful in interpreting measurements of variable error.

3.4 Transformed Variable Error. Distortions introduced in coordinate transformations will also affect patterns of variable error as the error is passed from one coordinate frame to another. Noise at the input will be reshaped by an inaccurate coordinate transformation such that a distorted transformation may introduce anisotropy to otherwise balanced input noise. In our model system, the improper computation of target distance would create laterally oriented variable-error ellipsoids from isotropic input noise (see Figure 6A). Furthermore, the combination of bias, noise, and local distortions can create diverse patterns of orientation in each of the three measures of error. Figure 6B indicates the patterns of error seen for our model system in the combined presence of (1) radially oriented input noise that increases with the square of the target distance, as would be expected from a binocular estimate of target distance and direction, (2) rightward bias in the internal representation of target direction, and (3) distortion in the polar-to-Cartesian transformation as defined by equation 3.4. One can see from this example that local distortions later in the transformation can reshape anisotropic input noise in a workspace-dependent fashion.

To understand the effect of a given transformation on the shape of a variable-error distribution, one must know the Jacobian matrix of the transformation in question (McIntyre et al., 1997):

$$S_{out} = J^T S_{in} J, \quad (3.5)$$

where S_{in} and S_{out} are the input and output covariance matrices. The linear estimation of local distortion provides a direct estimate of this Jacobian matrix. The calculation of both variable error and local distortion can therefore be useful in identifying the steps in a sensorimotor transformation.

Consider, for example, hypothetical measurements of variable error in the input and output of our model system. Differences between the input and output distributions are ambiguously related to either a distortion introduced in a coordinate transformation or to additive noise at an intermediate step along the pathway. In the former case, the transformation error will also be evident in the measurement of local distortion. In fact, by combining measurements of variable error and local distortion, one may

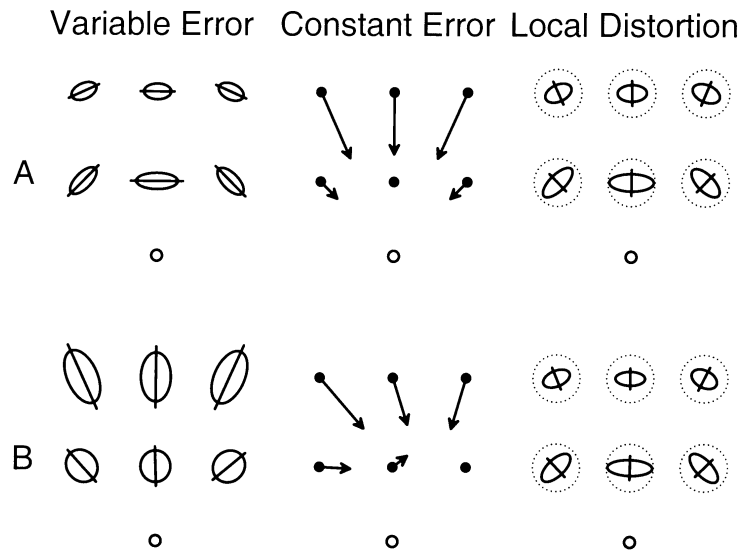


Figure 6: (A) Patterns of constant error, variable error, and local distortion induced by an incorrect scaling and offset in target distance for the transformation from polar to Cartesian coordinates at the output. Isotropic input noise is reshaped by the radial contraction, resulting in a lateral pattern of variable errors. For this simple and unique distortion, all three measurements of error provide congruent evidence for the internal polar coordinate system. (B) Combined effects of three different sources of error: noise in the estimate of distance that increases with the square of the distance, linear distortion and bias in the transformation from polar to Cartesian coordinates, and bias in X and Y. The three different measurements may show three different spatial patterns. The presence of bias can tilt the constant error vectors away from the origin of the intrinsic coordinate system. The anisotropic variability of the input is reshaped by the local distortion in the erroneous coordinate transformation. The measurement of local distortion is relatively independent of bias and noise that are injected into the system.

be able to identify specific representations of the target position that are not apparent in the output. By passing the known or measured input variance through the measured local distortion transformation, a prediction of the resulting output variability can be made. Features of the measured output variability that are seen in the predicted distribution can be attributed to coordinate transformations along the sensorimotor pathway. Patterns of variability not accounted for in the prediction would reflect noise added to the system at intermediate steps, giving evidence for an additional internal reference frame.

3.5 Neural Implementations. We have presented an idealized conception of sensorimotor processing in which data representations and coordinate transformations are distinct. Under this idealized framework, we have associated output variability with noise added to any or all of the data representations or in the execution of the motor output. For instance, noise could arise from the variability of the frequency of discharge of action potentials or from the variability of postsynaptic potentials. Conversely, we have attributed patterns of constant error or distortion to errors in transformations. In a neural circuit, distortions may arise from inaccuracies in the transmission or fusion of signals arising from separate neural pathways. These inaccuracies may, for example, arise from inappropriate tuning of synaptic weights within the circuitry, or they may reflect inherent limitations on the complexity of transformations that may be represented by a neuronal network.

It is likely, however, that many or all neural mechanisms manifest properties of both internal representations and transformations within the same circuitry. Memory storage provides a good example of this mix. Logically, the storage of a target position in memory would be described as an internal representation. One can expect that noise will increase over time as the memory of the target position fades. Drift might also occur, which would show up as time-dependent increases in measurements of constant error. Memory storage may also exhibit properties of a transformation or distortion. For instance, the subject's responses may converge toward a nominal or average pointing location as the quality of information in memory storage diminishes. Such a decay would appear as a gradually increasing contraction in measurements of local distortion. Thus, memory storage may best be described as a combination of internal representations and data transformations, although an explicit transformation between coordinate systems may not exist. The evolution of all three types of error (variable error, constant error, and local distortion) for different imposed delays may provide insight into the neural mechanisms that underlie the memory processes. The conceptual divide between representation and transformations can be a useful tool for describing these mechanisms even though neither of these constructs may exist in its pure form within the nervous system.

The methods described for analyzing errors must be used appropriately, so as not to ignore the assumptions underlying the analysis. For instance, the measurement of local distortion is precisely that: a local approximation of a global function. In essence, we are estimating the spatial derivative of the global transformation. The global function cannot be uniquely determined from a given derivative, and different global transformations might lead to similar patterns of local distortion. In addition, distortions at different levels along the sensorimotor chain will add. A blind calculation of the local distortion eigenvectors will not necessarily align with any of the internal reference frames. A similar caution applies to the analysis of variable error through the use of principal component analysis (PCA). As illustrated in

Figure 4, different sources of noise may add, leading to eigenvectors of the covariance matrix that do not align with any of the internal data representations. Furthermore, PCA assumes that the underlying coordinate axes are orthogonal. Violation of this assumption will also generate principal axes in the covariance matrix that would be misleading if blindly applied. The backward identification of a sensorimotor process based on measurements of error is thus ill posed. A more appropriate use of these methods is to test specific hypotheses about the neuronal process. Given a model of the transformations involved, one can predict the patterns of errors that will be seen at the output and compare these predictions with experimental results.

4 Experimental Methods

Subjects performed a pointing task to remembered visual targets presented by a robot in 3D space. The subject sat in a dimly lit room in front of a black table and backboard. The subject placed the index finger at a specified starting position, indicated by an upraised bump on the tabletop. A target LED was positioned by a robot at a specific 3D location, illuminated for 2 s, and then removed. After a programmed delay, an audible beep signaled to the subject to perform the pointing movement. The subject was instructed to place the tip of the index finger so as to touch the remembered position of the target LED. The subject was allowed 2 s to execute the pointing movement and hold the finger at the remembered target position. After a second beep, the subject returned the finger to the starting position in preparation for the next trial. Movements were recorded by an Elite 3D tracking system with a resolution of approximately 0.5 mm RMS. The final pointing position for each trial was calculated as the average final position over the last 10 samples (100 msec).

Subjects performed trials in blocks of 45 trials, each block lasting about 15 min. In a single block of trials, target locations were restricted to a small region of the workspace. Eight targets were distributed uniformly on a 22 mm radius sphere, with a ninth target position located at the center. Each of the nine targets was presented five times within a given block, and subjects performed four blocks of trials to each workspace region, for a total of 180 trials per region.

Three workspace regions were tested, located slightly above shoulder level, 60 cm in front of the subject. The center workspace regions was located on the midline, while the left and right regions were located 38 cm to each side of the center. Two starting positions, left and right, were tested, located on the table top approximately 20 cm in front of the subject and 20 cm to either side of the midline.

Subjects were tested with two different delay durations, 0.5 and 5.0 s, and two lighting conditions. In the lighted condition, dim room lights allowed the subject barely to see the fingertip against the black background. For the dark condition, the target was presented with the dim lights on, but at

the moment of target extinction, the room lights were extinguished, leaving the subject to wait during the memory delay and perform the pointing movement in total darkness.

Five right-handed subjects performed a complete set of pointing trials after a 0.5 s delay, using the right hand and starting from the right position, to all three workspace regions in dim light (*light-short*). The same five subjects performed trials in darkness for a 0.5 s (*dark-short*) and 5.0 s (*dark-long*) memory delay. Two right-handed subjects pointed to targets in all three workspace regions after a 5.0 s delay, using the right arm and starting from the right side (*light-long*). Five different right-handed subjects pointed in darkness after a 5.0 s delay with the right hand starting from the left side (*right-left*). A third set of eight right-handed subjects pointed to the left and right target regions only in darkness after a 5.0 s delay, using the left arm and starting from the left side (*left-left*). The *dark-long* condition is also referred to as the *right-right* condition, indicating use of the right hand from the right starting position.

4.1 Data Analysis. Constant error vectors, computed as the average error over all nine targets within a single workspace region, were calculated for each workspace region as described in McIntyre et al. (1997):

$$e = \frac{1}{n} \sum_{i=1}^9 \sum_{j=1}^{n^i} p_j^i - t^i \quad (4.1)$$

where t^i is the 3D vector location of target i , p_j^i is the final pointing position for trial j to target i , and n^i and n are the number of valid trials to target i and the total number of valid trials to all nine targets, respectively. The 3D covariance estimated from data over all $k = 9$ targets is computed by Morrison (1990):

$$S = \frac{\sum_{i=1}^k \sum_{j=1}^{n^i} \delta_j^i (\delta_j^i)^T}{n - k}, \quad (4.2)$$

where the deviation $\delta_j^i = p_j^i - \bar{p}^i$ for trial j to target i is computed relative to the mean \bar{p}^i of trials to target i , not to the overall mean for all targets. The 3D covariance matrix S can be scaled to compute the matrix describing the 95% tolerance ellipsoid, based on the total number of trials n :

$$T_{0.95} = q \frac{(n+1)(n-k)}{n(n-q-k+1)} F_{0.05, q, n-q-k+1} S \quad (4.3)$$

where $q = 3$ is the dimensionality of the Cartesian vector space and $k = 9$ is the number of targets.

The local transformation matrix M was computed as the linear relationship that best describes the transformation between a target position (relative to the average target position) and the displacement of end point positions for pointing trials to that target (relative to the overall average endpoint position for all trials), as computed by linear-least-squares methods.

The linear estimation of the local transformation may contain rotation or reflections as well as a local expansion and/or contraction. The overall local transformation can thus be represented as the cascade of two components: a symmetric matrix A , representing the local distortion, and an orthogonal matrix R ,

$$\tilde{M} = RA. \quad (4.4)$$

The symmetric component A was computed from the eigenvectors and eigenvalues of the quantity $\tilde{M}^T \tilde{M}$ as follows:

$$A = W \begin{bmatrix} \pm\sqrt{\lambda_1} & 0 & 0 \\ 0 & \pm\sqrt{\lambda_2} & 0 \\ 0 & 0 & \pm\sqrt{\lambda_3} \end{bmatrix} W^T \quad (4.5)$$

where

$$\tilde{M}^T \tilde{M} = W \begin{bmatrix} \lambda_1 & 0 & 0 \\ 0 & \lambda_2 & 0 \\ 0 & 0 & \lambda_3 \end{bmatrix} W^T \quad (4.6)$$

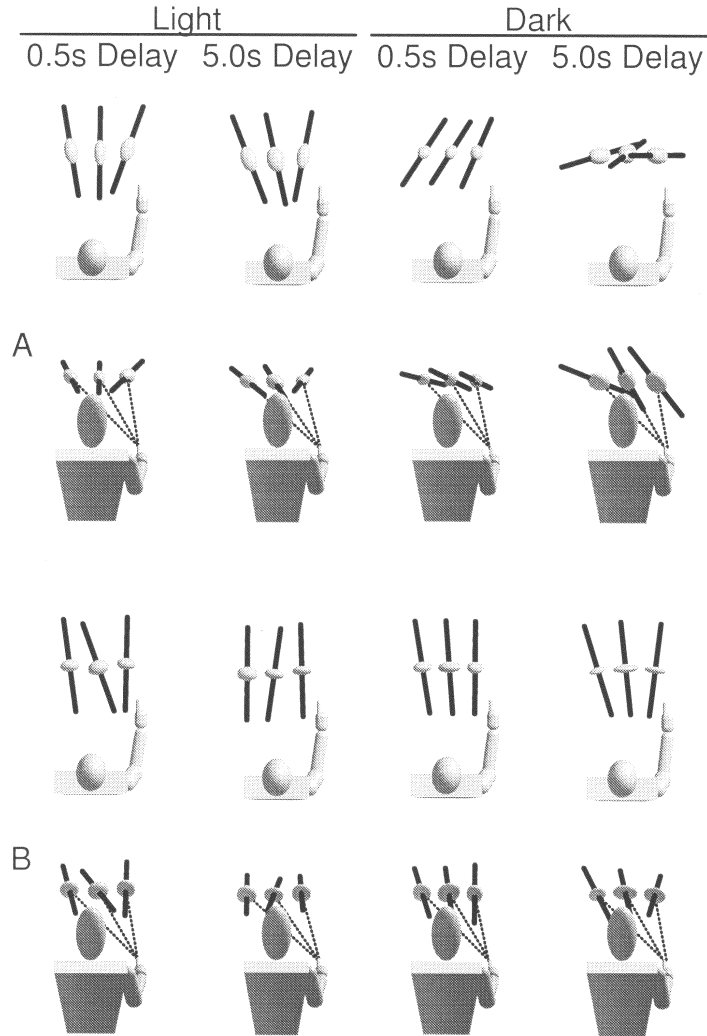
and W is thus the matrix of eigenvectors for the matrix $\tilde{M}^T \tilde{M}$. By judiciously selecting the signs of the roots in equation 4.5 so as to match the signs of the corresponding eigenvalues of \tilde{M} , reflections in the local transformation, if any, were included in the symmetric component A , and the orthogonal matrix R represents a rotation around a single axis. For A nonsingular, the matrix R is given by

$$R = MA^{-1}. \quad (4.7)$$

Expansion or contraction in the local transformation can be described by the matrix we call the local distortion, defined as

$$\Lambda = M^T M, \quad (4.8)$$

where the square root of the eigenvalues of Λ indicates the amount of expansion or contraction of output vectors along the eigenvectors of Λ (an eigenvalue equal to 1 implies no local distortion in that direction). The local distortion matrix can be plotted as an oriented 3D ellipsoid, where the major and minor axes indicated the directions of maximal and minimal expansion.



5 Experimental Results

Measurements of variable errors and local distortion showed anisotropic patterns for error that varied systematically as a function of workspace location. Figure 7 summarizes the patterns of variable error (A) and local distortion (B) observed for two memory delays and two lighting conditions. The data in this figure represent the average responses computed across subjects for each memory delay and lighting condition. In Figure 7A, each ellipsoid represents the combined 95% tolerance ellipsoid for pointing to

all nine targets within each workspace region. For pointing in the light, the axes of maximum variability for the computed variable-error ellipsoids, as indicated by dark bars passing along the major axis of each ellipsoid, converge toward the head of the subject. These data indicate a viewer-centered reference frame for the representation of the final pointing position when vision of the fingertip is allowed. A more detailed examination (data not shown) showed that this reference frame was independent of the starting hand position and the effector arm (McIntyre et al., 1997). In darkness, the major axes of the variable-error ellipsoids do not converge, and thus do not indicate a well-defined reference frame for the final pointing position when the fingertip is no longer visible.

Average local distortion ellipsoids for all subjects are presented in Figure 7B, where the axis of maximum contraction (third eigenvector) is indicated by dark bars. Local distortion measurements show a spatial organization that is common to both lighting conditions and memory delays and is more consistent than the pattern of variable errors seen for movements in the dark. For both lighting conditions, the minor axes of the local distortion ellipsoids point toward the subject, to a location situated somewhere between the eyes and the right shoulder.

To test for factors affecting the spatial orientation of pointing errors in the dark, we varied the starting position of the hand and the hand (left or right) used to perform the pointing task. Figure 8 shows the results of experiments with different starting positions and effector arms for pointing with a long delay in the dark. It can be seen that patterns of variable error differ according to the workspace region, the effector arm, and the starting hand position. Viewed from above, the variable-error ellipsoids in-

Figure 7: *Facing page.* Average variable errors (A) and local distortion (B) across subjects for two lighting conditions and two delays, viewed from above and perpendicular to the plane of movement. Small crosses indicate the starting position of the hand. (A) Ellipsoids represent the 95% tolerance region calculated from the matrix of variance and covariance, and the black bars indicate the axis of maximum variability. Dark line segments indicate the direction of the major eigenvector computed for the tolerance ellipsoid. For movements in the dark, a pattern of major eigenvector rotations upward and away from the starting position emerges in the ensemble averages, in comparison to head-centered eigenvector directions seen in the light. (B) Ellipsoids indicate the local distortions induced by the sensorimotor transformation, as estimated by a linear approximation to the local transformation. The unit sphere indicates the ellipsoid corresponding to an ideal, distortion-free local transformation. Dark bars indicate the direction of the third (minor) eigenvector, indicating the axis of maximum local contraction. Under all lighting conditions, axes of maximal contraction point toward the subject. Note the change of scale for ellipsoids viewed in the plane of movement.

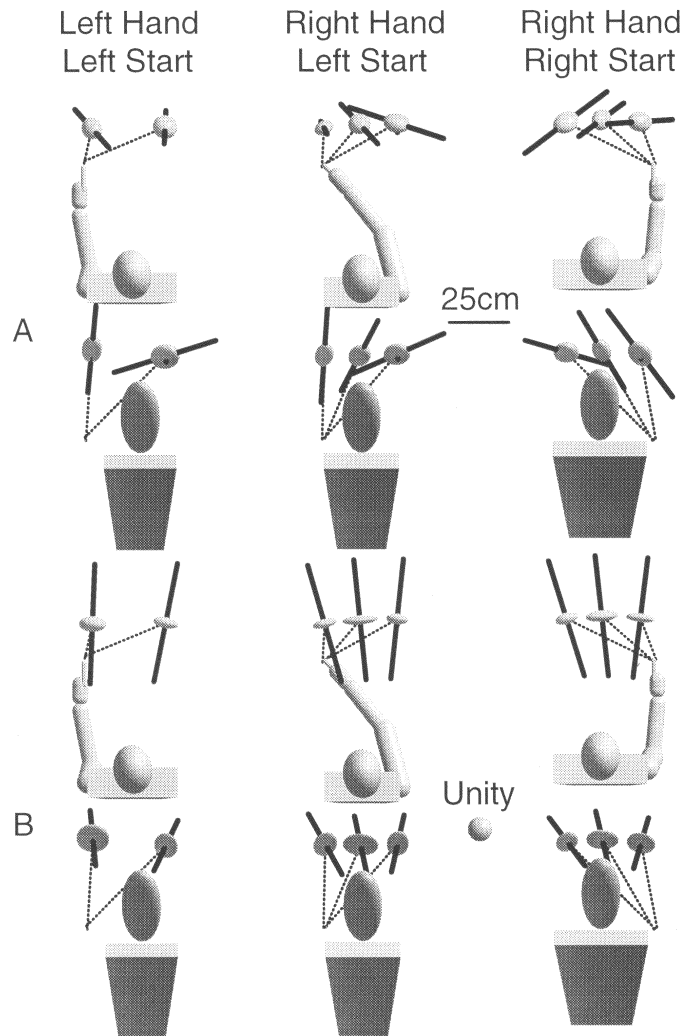


Figure 8: Effects of workspace region and movement starting position on estimates of variable error (A) and local distortion (B). The orientation of the variable-error ellipsoids is affected by the relative starting position of the hand but not by the hand used to perform the pointing. Axes of maximum contraction are biased slightly toward the side of the effector hand, independent of the starting hand position.

dicating a lateral distribution that rotates as the workspace location shifts from left to right. When viewed in the plane of movement (the plane containing the two starting positions and the center target location), the variable-error ellipsoids tend to rotate away from the line of movement in a pattern that is mirror symmetric for the right versus left starting position. In contrast, the minor axes for the measurements of local distortion are relatively unaffected by changes in the starting hand position. However, the axes of maximum contraction are biased toward the shoulder of the effector arm, independent of the starting position of the hand.

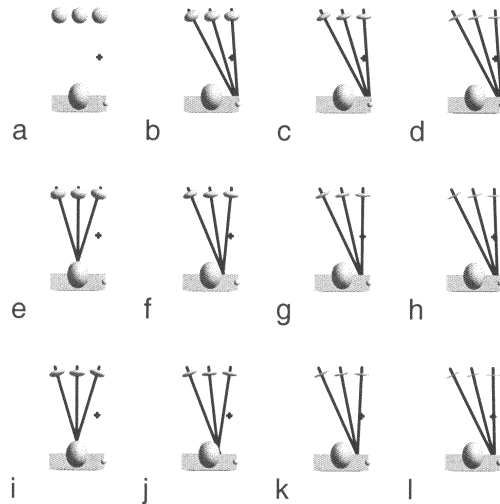
6 Simulations

The experimental results demonstrate a pattern of errors that at first glance do not point to a clearly defined reference frame for movements in the dark. The major axes of variable errors do not converge to a single origin, in contrast to the clearly viewer-centered errors seen in the light. Furthermore, the minor axes for measurements of local distortion, while clearly body-centered, do not point to a logically defined anatomical origin. However, distortions introduced at different stages in a sensorimotor chain combine to produce an overall local transformation in a manner that is not always intuitively obvious. Furthermore, distributions of errors that arise early in the sensorimotor pathway will be reshaped by distortions that occur in later steps of the transformation. We hypothesized that the reshaping and reorientation of variable-error ellipsoids observed for long delays in the dark may have been due entirely to the anisotropic distortions that develop in the sensorimotor transformation during the memory delay period. To test this hypothesis, we performed a set of simulations to see whether (1) a contraction of data along a shoulder-centered or a head-centered axis, or a combination of the two, can explain the observed patterns of local distortions and (2) whether local distortions in the target to end point mapping can explain the changes seen in the variable-error ellipsoids when movements are performed in the dark.

To this end we synthesized local transformation matrices M_v and M_a corresponding to local distortions aligned with the eyes and the shoulder, respectively. Each distortion was characterized by the unit vector v_0 parallel to the line from the designated origin to the center target position for a given workspace region and the amount of distortion (λ_v and λ_a) along this axis. The off-axis distortion eigenvalues were set to unity, and the simulated local transformations had no rotational component or reflections. The simulated local transformation can thus be computed as:

$$M = W \begin{bmatrix} \lambda_{on} & 0 & 0 \\ 0 & \lambda_{off} & 0 \\ 0 & 0 & \lambda_{off} \end{bmatrix} W^T \quad (6.1)$$

A. Simulation



B. Measured

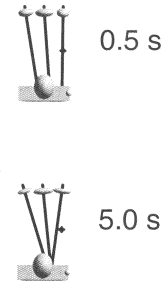


Figure 9: Simulation of net visuomotor transformations resulting from a cascade of two local distortions: one with an anisotropic contraction of end point positions along a head-centered direction and the second with a similar contraction along a shoulder-centered axis. In panel A, a-i represent the net local distortion at the output for different levels of contraction in each of the component steps. Starting from no distortion in either component for the upper left panel, shoulder-centered contraction increases from 1.0 on the left to 0.6 on the right, while head-centered distortion increases from 1.0 on the top to 0.6 on the bottom. To facilitate comparisons, the measured local distortion for pointing in the dark (see Figure 7) is presented in panel B.

where

$$W = [v_0 \quad v_1 \quad v_2] \quad (6.2)$$

is a orthogonal matrix formed from the desired major or minor axis v_0 and two mutually orthogonal unit vectors v_1 and v_2 lying in the plane perpendicular to v_0 . The net local transformation for a serial organization of eye-centered and then shoulder-centered distortion is given by

$$M_{net} = M_a M_v. \quad (6.3)$$

Figure 9A shows the simulated distortion ellipsoids for different combinations of head-centered and shoulder-centered contraction. In the grid, shoulder-centered contraction increases from left to right (λ_a varies from

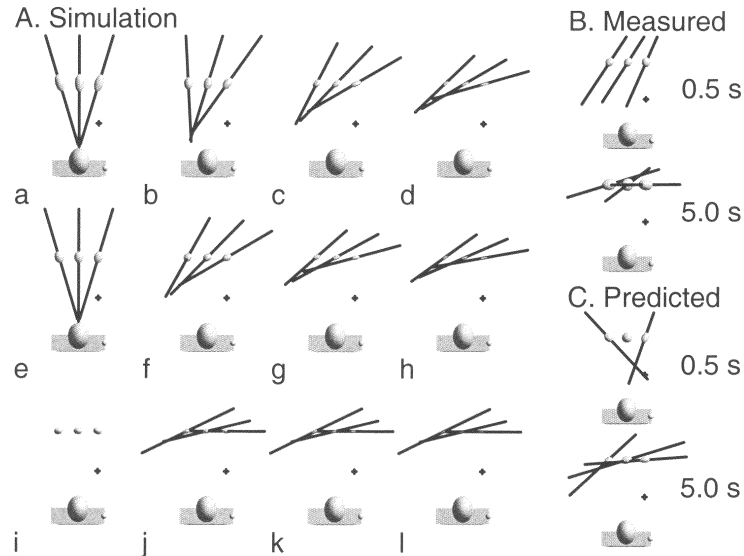


Figure 10: (A) Simulation of variable-error ellipsoids for each of the computed local transformations shown in Figure 9, viewed from above. Input variance for each workspace is taken from measurements of variable errors for pointing in the light with a short memory delay. (B) Average measured variable error for pointing in the dark (from Figure 7). (C) Simulated viewer-centered input noise transformed by the average local distortion measured for movements in the dark. Simulations e, f, and h, capture the qualitative features of the measured and predicted variable-error ellipsoids for a 5.0 s delay, but not for a 0.5 s delay.

1.0 to 0.6), while head-centered contraction increases from top to bottom (λ_v varies from 1.0 to 0.6). It is evident, as expected, that neither source of distortion alone can predict the actual measured transformation shown in Figure 9B. Axes of maximum contraction would point directly at the shoulder for a shoulder-centered-only distortion (top row) while viewer-centered distortions (left column) would produce a strictly head-centered pattern of orientations. The combined effect of both types of distortion, however, can create an intermediate center of rotation, with Figure 9h showing reasonably good correspondence with the average measured values.

Figures 10 through 12 show the predicted variable-error ellipsoids for each of the simulated local distortions shown in Figure 9, assuming a viewer-centered input distribution. A purely viewer-centered input variance S_v was computed using eigenvalues ($\lambda_{on} = \sqrt{25.0}$, $\lambda_{off} = \sqrt{12.0}$) similar to those found for movements in the light with a 5.0 s delay (see Figure 7). The predicted end point variable error for each simulated distortion from

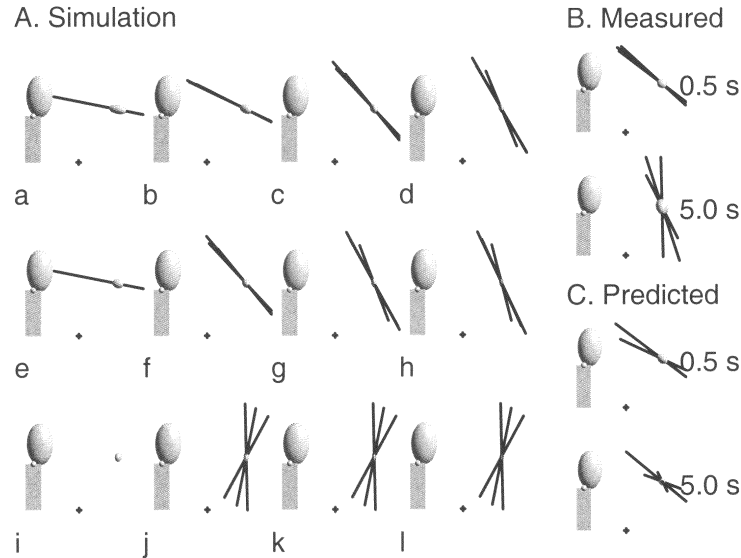


Figure 11: The same simulated and measured data as in Figure 10, viewed from the side. Simulations f and h show features qualitatively similar to the measured data in panel C, with variable-error ellipsoids pointing above the head of the subject.

Figure 9 was computed by inserting S_v and M_{net} into equation 3.5:

$$S = M_{net}^T S_v M_{net} \quad (6.4)$$

$$S = M_a^T M_v^T S_v M_v M_a. \quad (6.5)$$

For comparison, the average variable-error ellipsoids for movements in the dark (also from Figure 7) are included in panel B of each figure. In addition, a second simulation is included in panel C, in which the viewer-centered variable-error ellipsoid S_v was transformed by the average measured local distortion \tilde{M} for delayed movements in the dark (from Figure 7). Viewed from above (see Figure 10) and from the side (see Figure 11), transformations of the viewer-centered variable error by either the simulated or the measured local distortion capture two of the main qualitative features of the measured variable error. Viewed from above, there is a shift from a converging pattern of variable-error axes toward the subject to a lateral pattern of variability, as both the combined head- and shoulder-centered contraction increases in the simulation, and in the measured and predicted variable errors for the long delay in the dark. Viewed from the

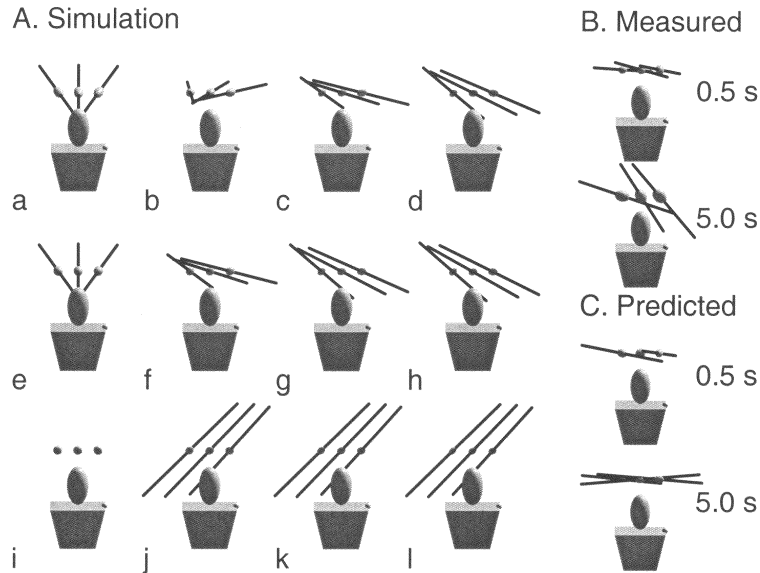


Figure 12: The same simulated and measured data as in Figure 10, viewed perpendicular to the movement plane. Neither the simulated data in A nor the computed variance distributions in C reflect the starting-point dependence evident in B and in Figure 8.

side, the simulated head and shoulder contraction also predicts the upward rotation of the major eigenvectors toward the vertical.

The simulations do not, however, reproduce all of the qualitative features of the measured variable-error ellipsoids. The major eigenvectors of variable errors measured for a short delay do not seem to converge, in contrast to the simulated patterns seen in Figure 10. Furthermore, when observed from a viewpoint perpendicular to the movement plane (see Figure 12), the simulations that best reproduce the data in the other planes do not reproduce the characteristic rotation of the variable-error ellipsoids away from the starting hand position. On the other hand, neither does the transformation of the viewer-centered input variance by the measured distortion, shown in Figure 12C. Thus, the effect of starting hand position (or movement direction) reflects an additional source of noise added to the sensorimotor pathway, rather than a distorted transformation into a hand-centered representation of the upcoming movement.

Figures 13 and 14 show the effects on the simulated variable-error ellipsoids of adding increased noise along the axis of movement of the hand (which we will refer to as hand-centered noise). In these figures, head-centered contraction is held constant at $\lambda_v = 0.8$ while shoulder-centered

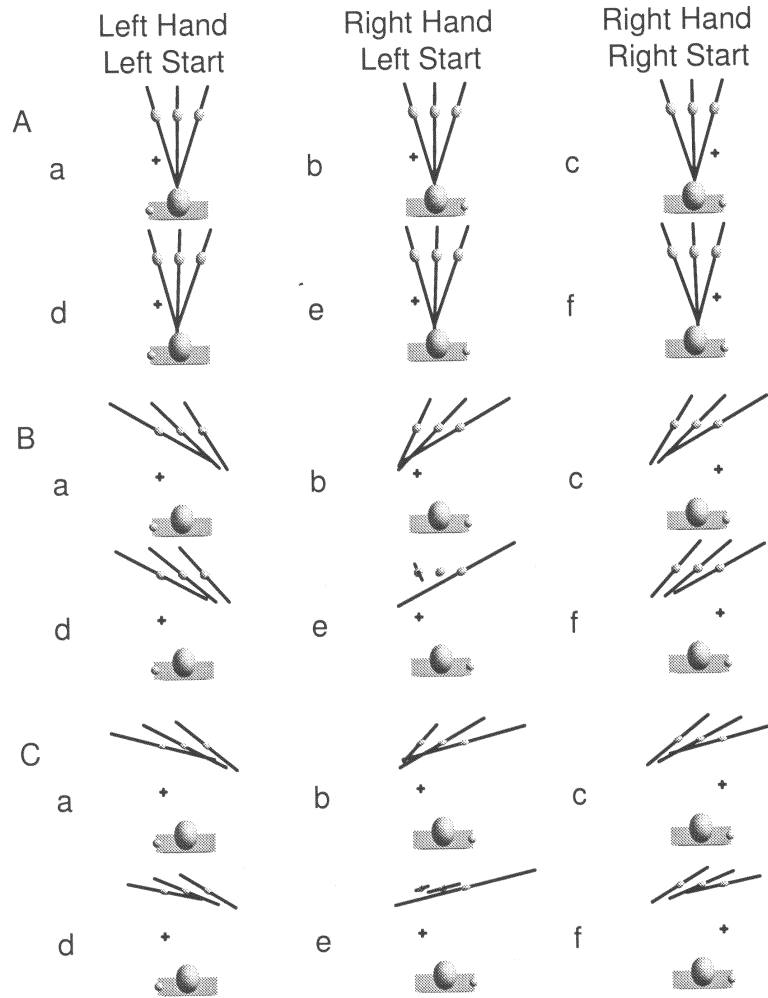


Figure 13: Simulation of variable-error ellipsoids for each of the computed local transformations, with the addition of anisotropic noise along the line from the initial hand position to the final end point position. Viewer-centered contraction is held constant at 0.8. Shoulder-centered contraction increases from 0.0 in A to 0.6 in C. Additive hand-centered noise is 0 mm (S.D.) in the first row of each group (a-c) and 6 mm in the second (d-f). For up to 6 mm of hand-centered noise, the patterns of variable error are dominated by the viewer-centered input noise and the head- and shoulder-centered contraction, resulting in the lateral pattern of major eigenvectors seen for human subjects.

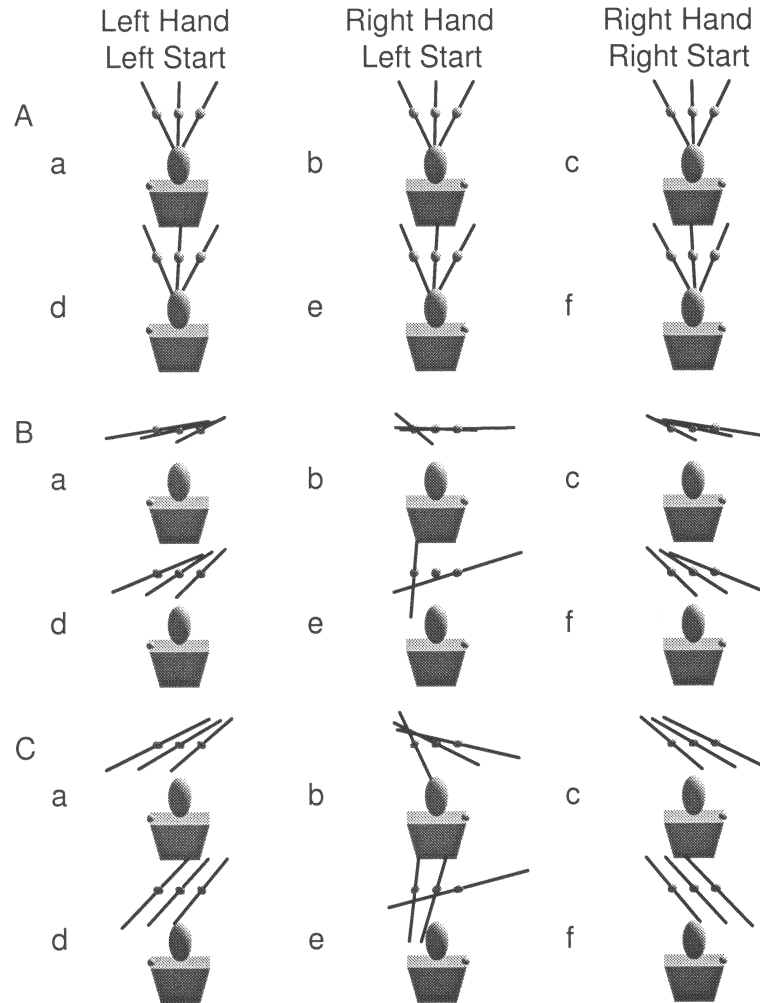


Figure 14: Same as Figure 13, viewed perpendicular to the movement plane. When hand-centered noise is absent (a-c in each group), the pattern of variable errors depends on the effector hand, not the starting hand position. Increasing levels of hand-centered noise (d-f) can generate patterns that depend on hand starting position, as seen in Figure 8.

contraction increases from 0.0 (A) to 0.6 (C). Variance along the line from starting to final pointing position is $\sigma_h = 0$ for panels a through c in each group and $\sigma_h = 6$ mm for panels d through f. Viewed in the horizontal plane, the pattern of major eigenvectors for variable error is dominated by

viewer-centered input noise and the head- and shoulder-centered contractions, resulting in a lateral pattern of major eigenvectors as the shoulder-centered contraction increases. One can see how the parallel variable-error axis seen for the 0.5 s delay in the dark might result from a moderate amount of head-centered and shoulder-centered contraction plus additional noise along the hand movement axis. With the shoulder-centered distortion fixed at $\lambda_a = 0.8$ (see Figure 13B), increasing the amount of hand-centered noise (panel f versus c) causes the major eigenvector to swing toward the left shoulder, and the convergence of the eigenvectors decreases.

Figure 14 demonstrates how the added hand-centered noise can cause the variable-error major axes to point away from the starting hand position when viewed in the plane of movement. The simulation of noise along the line from the left starting position produces a mirror effect of starting position when viewed in the same plane. Note that the effects of hand-centered noise not seen in the orientation of the variable major axis (see Figure 14A, panels d–f) can be revealed by increasing levels of body-centered local contraction (see Figures 14B and 14C, panels d–f). Thus, a given level of hand-centered noise will have a greater effect on the direction of the variable-error major eigenvector as local contraction increases. It is therefore possible that the effects of starting hand position on variable error may in fact be present for pointing in the dark for all memory delays, but that these effects are not revealed in the measurement of variable error until a longer memory delay generates a sufficiently high level of contraction in depth.

The simulations depicted in Figures 10 through 14 do not reproduce exactly the measured patterns of variable error. For example, there is not a single combination of viewer-centered contraction, shoulder-centered contraction, and hand-centered noise that can match precisely the features of the measured variable error from all viewpoints simultaneously. Nevertheless, these simulations demonstrate how the different qualitative features can be achieved by varying the weight of the different sources of error. Discrepancies between the simulations and the measured data may arise from varying relative weights for the different error sources among different subjects included in the average. On the other hand, some additional differences between the simulations and measurements, such as the counterclockwise rotation of the variable-error major axis viewed in the movement plane (see Figure 8), may be due to additional features of the sensorimotor process that have yet to be accounted for.

7 Discussion

In this article we have formally described how various sources of error added along a sensorimotor pathway can combine to generate patterns of errors in the motor output of a pointing task. Conversely, we have shown how measurements of errors at the output can reveal properties of the underlying neural circuitry. We have used these concepts to model the behavior

of human subjects for pointing to remembered 3D targets. Although this particular model may not provide the only explanation of the observed behavior, the results of this study demonstrate how the cumulative effects of noise and distortion lead to patterns of variable error that might not be otherwise intuitively obvious. We propose that computational analyses of the type described here may be useful in understanding electrophysiological and psychophysical data and will lead to experimentally verifiable models of biological sensorimotor systems, as we will discuss below.

The measure of local distortion described in this article provides a useful complement to the measures of variable and constant error. First, because it is based on local rather than global linearization methods, it is much less sensitive to nonlinearity in the sensorimotor pathways. The validity of the measurement of local distortion requires only that the overall transformation be smooth. Thus, the calculation of local distortion will be appropriate even if a global linearization is not (Bookstein, 1992). Furthermore, spatial patterns of local distortion for these experiments have proved to be more consistent across subjects than are measures of constant error (McIntyre et al., 1998). This indicates that local contraction, rather than global bias, is an invariant property of pointing behavior. Finally, the calculation of local distortion allows for a better understanding of observed patterns of variable error. As shown by the simulations presented above, patterns of measured variable errors may be due to inaccurate coordinate transformations between reference frames rather than to noise added to additional intermediate internal representations.

In the experiments described here, the consideration of local distortion in addition to measures of constant and variable error provided a clearer picture of the underlying neural mechanisms. By comparing the experimental results and the simulations presented here, one can conclude that much of the difference in variable errors observed for pointing in the dark versus the light can be attributed to distortions introduced in the transformation of the visual acquired target location to the final finger position. This transformation includes effects contributed by the storage of the desired pointing position, as indicated by the increasing effect of local distortion for longer memory delays (McIntyre et al., 1998). However, an additional source of noise is required to account fully for the dependence of variable-error orientation on the starting hand position, which is likely to be related to the direction of movement. In the following paragraphs we consider the significance of the identified viewer-centered noise, head- and shoulder-centered distortion, and hand-centered variability.

The compression of responses toward the mean is a general phenomenon known as a central tendency or range effect (Poulton, 1981). A general compression of the data toward the center would not in itself be very interesting; however, when the central tendency is anisotropic, as in this study, the anisotropy can indicate the separation of spatial information into independent channels, each of which exhibits its own range effect. In our

experiments, the direction of maximum contraction is almost, but not quite, aligned with the viewer-centered axes of maximum variability observed for pointing in the light. This behavior suggests a Kalman filter type of processing in which the pointing response is the weighted sum of input signals and an “average” response, and in which the weight given to each input channel is determined by the expected noise in that channel. Because binocular estimates of distance are noisier than estimates of target direction, one would expect that the contraction toward the central value would be stronger in a radial direction. Furthermore, as noise increases in the stored representation of the target position, contraction should also increase. This appears to be the case for increasing memory delays in the dark (McIntyre et al., 1998).

It might seem therefore that the anisotropic contraction can be attributed to processing of the visual input. Foley (1980) found that the slope of perceived versus actual target distance is consistently less than unity for a variety of different estimation tasks. Gogel (1973) proposed that the central nervous system computes target distance as a weighted sum of different inputs (e.g., stereodisparity, vergence, accommodation), including a “specific distance” toward which the estimate is biased in the absence of adequate sensory cues. Contractions of pointing positions may reflect the bias toward the specific distance postulated by Gogel, and we propose further that the weighting of different visual cues may be determined by the expected variability in each channel. For pointing, however, one cannot predict the rotation of the local distortion ellipsoid toward the effector arm by the filtering of viewer-centered noise mapped onto an isotropic internal representation of the target position. Noise in the binocular acquisition of the target should not depend on the effector arm. Observed patterns of local distortion would, on the other hand, be consistent with a mapping of the target position into a shoulder-centered reference frame, followed by a Kalman-type filter applied in this transformed coordinate system.

There is, in fact, also evidence for arm-centered local contraction in pure motor tasks. When pointing to kinesthetically presented targets, subjects tend to underestimate the perceived target distance from the shoulder (Baud-Bovy & Viviani, 1998). These data indicate a polar representation of the target position in separate channels of shoulder-centered distance, azimuth, and elevation, as has previously been proposed (Soechting & Flanders, 1989a; Lacquaniti et al., 1995). Local distortion data from the current experiment are, however, also consistent with a distorted transformation into arm segment orientations (arm and forearm azimuth and elevation; Soechting & Flanders, 1989b) or intrinsic shoulder and elbow angle components. This is because the direction to the fingertip is determined primarily by the two shoulder angles, while the distance from shoulder to finger is largely determined by the degree of elbow extension. Note that it is difficult to differentiate between these models because they are intrinsically related. An underestimation of shoulder-centered target distance would generate an underestimation of elbow extension and vice versa (Bennett & Loeb, 1992).

Indeed, Baud-Bovy and Viviani (1998) observed slopes consistently less than unity in the regression of perceived versus actual arm elevation for pointing to a kinesthetically presented target. Nevertheless, these authors have argued for a spherical target position representation centered at the shoulder, rather than a limb orientation or joint angle representation, based on the analysis of noise correlation for different hypothesized coordinate frames.

Thus, a number of studies have identified a viewer-centered reference frame for visually guided pointing to visually presented targets (Soechting, Helms Tillery, & Flanders, 1990; McIntyre et al., 1997). Conversely, an arm-centered reference frame has been identified for pointing to kinesthetically presented targets (Baud-Bovy & Viviani, 1998). In the experiments presented here for pointing to visually presented targets without visual guidance, our measurements of local distortions indicate an intermediate reference frame with an origin located between the eyes and shoulder. Using different methods, Soechting and colleagues (Soechting et al., 1990; Helms Tillery, Flanders, & Soechting, 1991; Flanders, Helms Tillery, & Soechting, 1992) have also identified an intermediate reference frame related to both the visual target and the effector arm. Our analysis provides a more explicit explanation for this intermediate representation. Simulations show how the cascading effects of two transformations, one centered at the eyes and the second at the shoulder, can predict the intermediate center of rotation seen in the data.

Data from three different experiments support the hypothesis of a two-stage transformation, with a gradual passage from viewer-centered to shoulder-centered coordinates. For pointing to continuously visible targets, without vision of the hand, Carrozzo, McIntyre, Zago, and Lacquaniti (1999) found local contraction axes that point toward the subject but that are not necessarily biased toward the shoulder. Although Baud-Bovy and Viviani (1998) did not explicitly measure local distortion, in their experiments on pointing to kinesthetic targets, the observed convergence of the minor axes for the variable-error ellipsoids toward the shoulder of the effector arm is consistent with a local distortion (local contraction) in a shoulder reference frame. In our experiments for pointing to remembered visual targets, we found significant local distortion for both lighting conditions and memory delays, but the bias toward the effector arm is most readily apparent for the longer delay in the dark. Nevertheless, the bias toward the shoulder for pointing to visual targets (see Figure 7) does not appear to be as strong as that seen for pointing to kinesthetic targets (see Baud-Bovy & Viviani, 1998, Figure 7). The ensemble of these results suggests that a visual target is first represented in a viewer-centered reference frame, with a contraction of perceived distances along the sight line, and then transformed into an arm-centered representation, with an associated distortion in the arm-linked reference frame. As the memory delay increases, the internal representation of the intended hand movement appears to decay in this arm-linked reference frame.

7.1 Implications for Neural Circuits. Anisotropies in the transformation process, particularly those arising from the decay in the memory of the target position, have meaningful implications for the neural mechanisms involved in sensorimotor transformations and memory. Anisotropic compression along an egocentric axis is a behavioral characteristic that one can search for within the neural networks of the brain, in much the same way that behavioral phenomena such as mental rotation (Georgopoulos, Lurito, Petrides, Schwartz, & Massey, 1989) and the two-thirds power law (Schwartz, 1994) have been observed in population vectors measured in M1. Evidence for egocentric compression within a specific neural representation of the target position would help to identify the structures that implement the sensorimotor transformations and short-term working memory. Note that the tuning curves of neurons in the superior parietal lobule of the monkey recorded during pointing to visual targets exhibit a body-centered contraction reminiscent of the radial contraction described here (Lacquaniti, Guignon, Bianchi, Ferraina, & Caminiti, 1995), suggesting a neural manifestation of the observed behavioral effects. In addition, neurological patients affected by optic ataxia, a disturbance of visuomotor coordination due to lesions of the interparietal sulcus and the superior parietal lobule, exhibit a specific deficit in pointing to a visual target (Perenin & Vighetto, 1988; Ratcliff & Davies-Jones, 1972) that consists of a pattern of local distortion qualitatively akin to the one we have reported here, although of much greater magnitude. Thus, this particular deficit may be an exaggeration of a relatively normal physiological process.

Known properties of a variety of different cortical areas provide a number of potential loci for the transformations and representations proposed here. Parietal cortex is replete with cells that combine information about eye, neck, arm, and hand positions, as is the case for premotor cortex (Anderson, Snyder, Bradley, & Xing, 1997; Boussaoud, 1995). Cells in LIP seem to code 3D space through the mechanism of gain fields, in which radial 2D receptive fields are modulated multiplicatively by a sigmoid function of depth. This representation mechanism could account for the anisotropic distortion between depth and direction observed for the final positions in our pointing task.

The anisotropic modification of the memorized target location (or intended movement end point) over the delay period argues for a parcelation of target position information into separate channels, each represented by a relatively independent set of memory-related neurons. In this light, end-point-position sensitive neurons, such as those found in parietal cortex area 5, become good candidates for the locus of the target position memory (Lacquaniti et al., 1995). On the other hand, uniform encoding of hand displacement direction, as has been postulated for area M1 (Georgopoulos et al., 1988), would be inconsistent with the anisotropic memory decay observed for movements in the dark. Although the vector coding scheme proposed for M1 separates movement distance from direction, the reference frame for

this system is the hand's initial position, not a body-centered origin. This is not to say that alternative representations situated upstream or downstream from the egocentric working memory would have no effect on the evolution of the stored target position over time. On the contrary, both the fact that hand-centered M1 neurons are active during memory delay periods (Smyrnis, Taira, Ashe, & Georgopoulos, 1992) and that noise tends to be greater along the axis of movement (Gordon, Ghilardi, & Ghez, 1994; Desmurget et al., 1997; McIntyre et al., 1998) indicate that a hand-centered representation of the intended limb displacement plays a detectable role in the representation of the upcoming movement. Furthermore, undistorted pointing when vision of the fingertip is allowed suggests that the visual representation of the target persists in memory during the delay period. Likewise, shifts in gaze direction during the memory delay period can affect the final pointing position, even when vision of the fingertip is prevented (Enright, 1995; Henriques, Klier, Smith, Lowy, & Crawford, 1998). These results suggest an ongoing influence of visuomotor inputs to the short-term memory of the target position or intended movement. Theoretical models suggest how neural networks might represent target locations simultaneously in different reference frames linked to different sensory modalities and/or motor outputs, and how coherence may be maintained between these different reference frames (Droulez & Berthoz, 1991; Pouget & Sejnowski, 1997). Nevertheless, in our experiments, distortion of the final end point positions along a head-shoulder axis increased in a time-dependent fashion during the memory delay period when there was no modification of the visual input, eye position, or body posture. We therefore postulate that the primary storage of the target position or intended movement during the memory delay is carried out in an egocentric representation of the final end point position.

Acknowledgments

This work was carried out under the auspices of the European Laboratory for the Neuroscience of Action. This work was supported in part by grants from the Italian Health Ministry, the Italian Space Agency ASI, the French space agency CNES, the Ministero della Università a Ricerca Scientifica Tecnologica, and Telethon-Italy.

References

- Andersen, R. A., Snyder, L. H., Bradley, D. C., & Xing, J. (1997). Multimodal representation of space in the posterior parietal cortex and its use in planning movements. *Ann Rev Neurosci*, *20*, 303-330.
- Baud-Bovy, G., & Viviani, P. (1998). Pointing to kinematic targets in space. *J Neurosci*, *18*, 1528-1545.
- Bennett, D. J., & Loeb, E. (1992). Error analysis, regression and coordinate systems. *Behav Br Sci*, *15*, 326.

- Berkinblit, M. B., Fookson, O. I., Smetanin, B., Adamovich, S. V., & Poizner, H. (1995). The interaction of visual and proprioceptive inputs in pointing to actual and remembered targets. *Exp Brain Res*, *107*, 326–330.
- Bookstein, F. L. (1992). Error analysis, regression and coordinate systems. *Behav Br Sci*, *15*, 327–328.
- Boussaoud, D. (1995). Primate premotor cortex: modulation of preparatory neuronal activity by gaze angle. *J Neurophysiol*, *73*, 886–890.
- Carrozzo, M., McIntyre, J., Zago, M., & Lacquaniti, F. (1999). Viewer-centered and body-centered frames of reference in direct visuo-motor transformations. *Experimental Brain Res*, *129*, 201–210.
- Darling, W. G., & Miller, G. F. (1993). Transformations between visual and kinesthetic coordinate systems in reaches to remembered object locations and orientations. *Exp Brain Res*, *93*, 534–547.
- Desmurget, M., Jordan, M., Prablanc, C., & Jeannerod, M. (1997). Constrained and unconstrained movements involve different control strategies. *J Neurophysiol*, *77*, 1644–1650.
- Droulez, J., & Berthoz, A. (1991). The concept of dynamic memory in sensorimotor control. In D. R. Humphrey & H. J. Freund (Eds.), *Motor control: Concepts and issues* (pp. 137–161). New York: Wiley.
- Enright, J. T. (1995). The non-visual impact of eye orientation on eye-hand coordination. *Vis Res*, *35*, 1611–1618.
- Flanders, M., Helms Tillery, S. I., & Soechting, J. F. (1992). Early stages in a sensorimotor transformation. *Behav Br Sci*, *15*, 309–362.
- Foley, J. M. (1980). Binocular distance perception. *Psychol Rev*, *87*, 411–435.
- Foley, J. M., & Held, R. (1972). Visually directed pointing as a function of target distance, direction and available cues. *Percept Psychophys*, *12*, 263–268.
- Georgopoulos, A. P., Kettner, R. E., & Schwartz, A. B. (1988). Primate motor cortex and free arm movements to visual targets in three-dimensional space. II. Coding of the direction of movement by a neuronal population. *J Neurosci*, *8*, 2928–2937.
- Georgopoulos, A. P., Lurito, J. T., Petrides, M., Schwartz, A. B., & Massey, J. T. (1989). Mental rotation of the neuronal population vector. *Science*, *243*, 234–236.
- Gogel, W. C. (1973). Absolute motion, parallax and the specific distance tendency. *Percept Psychophys*, *13*, 284–292.
- Gordon, J., Ghilardi, M. F., & Ghez, C. (1994). Accuracy of planar reaching movements. I Independence of direction and extent variability. *Exp Brain Res*, *99*, 97–111.
- Helms Tillery, S. I., Flanders, M., & Soechting, J. F. (1991). A coordinate system for the synthesis of visual and kinesthetic information. *J Neurosci*, *11*, 770–778.
- Henriques, D. P., Klier, E. M., Smith, M. A., Lowy, D., & Crawford, J. D. (1998). Gaze-centered remapping of remembered visual space in an open-loop pointing task. *J Neurosci*, *18*, 1583–1594.
- Lacquaniti, F. (1997). Frames of reference in sensorimotor coordination. In M. Jeannerod & J. Grafman (Eds.), *Handbook of neuropsychology* (Vol. 2, pp. 27–64). Amsterdam: Elsevier.

- Lacquaniti, F., Guigon, E., Bianchi, L., Ferraina, S., & Caminiti, R. (1995). Representing spatial information for limb movement: Role of area 5 in the monkey. *Cereb Cortex*, *5*, 391–409.
- McIntyre, J., Stratta, F., & Lacquaniti, F. (1997). A viewer-centered reference frame for pointing to memorized targets in three-dimensional space. *J Neurophysiol*, *78*, 1601–1618.
- McIntyre, J., Stratta, F., & Lacquaniti, F. (1998). Short-term memory for reaching to visual targets: Psychophysical evidence for body-centered reference frames. *J Neurosci*, *18*, 8423–8435.
- Merton, P. A. (1961). The accuracy of directing the eyes and the hand in the dark. *J Physiol*, *156*, 555–577.
- Morrison, D. F. (1990). *Multivariate statistical methods*. New York: McGraw-Hill.
- Perenin, M. T., & Vighetto, A. (1988). Optic ataxia: A specific disruption in visuomotor mechanisms. I. Different aspects of the deficit in reaching for objects. *Brain*, *111*, 643–674.
- Poulton, E. C. (1981). Human manual control. In V. B. Brooks (Ed.), *Motor control* (pp. 1337–1389). Bethesda, MD: American Physiological Society.
- Pouget, A., & Sejnowski, T. J. (1997). Spatial transformations in the parietal cortex using basis functions. *J Cog Neurosci*, *9*, 222–237.
- Prablanc, C., Echallier, J. F., Komilis, E., & Jeannerod, M. (1979). Optimal response of eye and hand motor systems in pointing at a visual target. I. Spatio-temporal characteristics of eye and hand movements and their relationship when varying the amount of visual information. *Biol Cybern*, *35*, 113–124.
- Ratcliff, G., & Davies-Jones, G. A. (1972). Defective visual localization in focal brain wounds. *Brain*, *95*, 49–60.
- Schwartz, A. B. (1994). Direct cortical representation of drawing. *Science*, *265*, 540–542.
- Sherrington, C. S. (1918). Observations on the sensual role of the proprioceptive nerve-supply of the extrinsic ocular muscles. *Brain*, *41*, 332–343.
- Smyrnis, N., Taira, M., Ashe, J., & Georgopoulos, A. P. (1992). Motor cortical activity in a memorized delay task. *Exp Brain Res*, *92*, 139–151.
- Soechting, J. F., & Flanders, M. (1989a). Errors in pointing are due to approximations in sensorimotor transformations. *J Neurophysiol*, *62*, 595–608.
- Soechting, J. F., & Flanders, M. (1989b). Sensorimotor representations for pointing to targets in three-dimensional space. *J Neurophysiol*, *62*, 582–594.
- Soechting, J. F., Helms Tillery, S. I., & Flanders, M. (1990). Transformation from head- to shoulder- centered representation of target direction in arm movements. *J Cog Neurosci*, *2*, 32–43.